RESEARCH ARTICLE

A family of horizon-penetrating coordinate systems for the Schwarzschild black hole geometry with Cauchy temporal functions

Christian Röken[1,2]

Abstract

We introduce a new family of horizon-penetrating coordinate systems for the Schwarzschild black hole geometry that feature time coordinates, which are specific Cauchy temporal functions, i.e., the level sets of these time coordinates are smooth, asymptotically flat, spacelike Cauchy hypersurfaces. Coordinate systems of this kind are well suited for the study of the temporal evolution of matter and radiation fields in the joined exterior and interior regions of the Schwarzschild black hole geometry, whereas the associated foliations can be employed as initial data sets for the globally hyperbolic development under the Einstein flow. For their construction, we formulate an explicit method that utilizes the geometry of—and structures inherent in—the Penrose diagram of the Schwarzschild black hole geometry, thus relying on the corresponding metrical product structure. As an example, we consider an integrated algebraic sigmoid function as the basis for the determination of such a coordinate system. Finally, we generalize our results to the Reissner–Nordström black hole geometry up to the Cauchy horizon. The geometric construction procedure presented here can be adapted to yield similar coordinate systems for various other spacetimes with the same metrical product structure.

✉ Christian Röken
croken@correo.ugr.es; croeken@uni-bonn.de

1   Department of Geometry and Topology, Faculty of Science, University of Granada, 18071 Granada, Spain

2   Lichtenberg Group for History and Philosophy of Physics, Faculty of Philosophy, University of Bonn, 53113 Bonn, Germany

🖄 Springer

Contents

1 Introduction

In a certain class of 4-dimensional Lorentzian manifolds, there exist preferred 2-dimensional submanifolds with induced metrics that are locally and conformally equivalent to the actual Lorentzian metrics. These submanifolds may be used to analyze the global causal structures of the underlying Lorentzian manifolds. For first applications of this approach to the Schwarzschild, Reissner–Nordström, and Kerr geometries, we refer the reader to, e.g., [5, 6, 15, 18, 23]. As can be seen, i.a., from these first applications, one of the most prominent examples of such preferred 2-dimensional submanifolds are the 2-surfaces containing the two double principal null directions in a Petrov type D solution of the vacuum Einstein field equations in general relativity [19, 38], which can be employed to study the causal structures of black hole geometries, for instance, by means of Penrose diagrams [10, 35]. In particular, this concept of analyzing the causal structures of 4-dimensional Lorentzian manifolds is especially useful in the context of global hyperbolicity, which is a specific condition on the causal structures of Lorentzian manifolds that gives rise to foliations by smooth, spacelike Cauchy hypersurfaces. Thus, it is relevant for the initial value formulation of the Einstein field equations (see, e.g., [8]), where one works with spacelike Cauchy hypersurfaces as initial data sets and derives solutions evolving this data forward and backward in time. Examples of such foliations of the maximal globally hyperbolic extensions of some spherically symmetric Lorentzian 4-manifolds by spacelike Cauchy hypersurfaces that are maximal or have constant mean curvature can be found in [1, 4, 12, 14, 30, 31, 37, 41].

In this work, we focus on an explicit construction procedure of global coordinate systems for a specific globally hyperbolic subset of the family of spherically symmetric vacuum geometries, namely the Schwarzschild black hole geometry, which are related to foliations by smooth, asymptotically flat, spacelike Cauchy hypersurfaces. The Schwarzschild black hole geometry is isometric to a subset of the maximally extended Schwarzschild geometry, viz. regions I and II [40], and may be used in order to describe the final equilibrium state of the dynamical evolution of the gravitational field of an isolated, nonrotating, uncharged black hole. More precisely, we present a 2-dimensional construction procedure of a new family of horizon-penetrating coordinate systems with Cauchy temporal functions (Cauchy coordinates) covering the

joined exterior and interior regions of the Schwarzschild black hole geometry, where we deform the geometric shape of the associated Penrose diagram from a trapezoid into a centrally symmetric diamond via affine as well as homotopy transformations, and formulate conditions for the determination of families of smooth functions foliating this diamond. These functions are identified with smooth, spacelike Cauchy hypersurfaces in the Schwarzschild black hole geometry, which are asymptotically flat at spacelike infinity, encounter the curvature singularity only asymptotically, and yield regular foliations across the event horizon. Hence, the labels of these hypersurfaces are Cauchy temporal functions on the Schwarzschild black hole geometry, and may serve as time variables of the aforementioned global coordinate systems. For the study of other families of horizon-penetrating coordinate systems related to foliations with similar boundary conditions and spatial slices with trumpet geometry, which, however, rely on different geometric construction procedures and do not, in general, yield foliations that cover the entire Schwarzschild black hole geometry up to the singularity, see [11, 22]. Having a coordinate system of the above type at one's disposal may be advantageous in the derivation of propagators for matter and radiation fields in a Schwarzschild black hole background geometry in the framework of (relativistic) quantum theory. Moreover, the foliations associated with these coordinate systems can be used as initial data sets for the globally hyperbolic development of the Schwarzschild black hole geometry under the Einstein flow, tracing its evolution over time.

The paper is organized as follows. In Sect. 2, we first recall the main geometrical and topological aspects of the Schwarzschild black hole geometry, present a derivation of compactified Kruskal–Szekeres coordinates, and study the corresponding Penrose diagram. We then give a brief account of the notions of Cauchy surfaces and time-type functions. Subsequently, in Sect. 3, we introduce our geometric method for the explicit construction of horizon-penetrating Cauchy coordinate systems for the Schwarzschild black hole geometry. We also prove that the level sets of the time variables of these coordinate systems are in fact Cauchy hypersurfaces. The details of a specific example based on an integrated algebraic sigmoid function are worked out in Sect. 4. In Sect. 5, we generalize our results to the Reissner–Nordström black hole geometry up to the Cauchy horizon. Finally, we conclude with a brief outlook on future research projects in Sect. 6.

2 Preliminaries

2.1 The Schwarzschild black hole geometry and compactified Kruskal–Szekeres coordinates

The Schwarzschild black hole geometry $(\mathfrak{M}, \boldsymbol{g})$ is a connected, smooth, globally hyperbolic and asymptotically flat Lorentzian 4-manifold with $\mathfrak{M}$ being homeomorphic to $\mathbb{R}^2 \times S^2$ and a spherically symmetric metric $\boldsymbol{g}$, referred to as the Schwarzschild metric, which constitutes a 1-parameter family of solutions of the vacuum Einstein field equations $\mathrm{Ric}(\boldsymbol{g}) = \boldsymbol{0}$. In the standard Schwarzschild coordinates $(t, r, \theta, \varphi) \in \mathbb{R} \times \mathbb{R}_{>0} \times (0, \pi) \times [0, 2\pi)$, this metric takes the form [36]

$$g = \left[1 - \frac{2M}{r}\right] dt \otimes dt - \left[1 - \frac{2M}{r}\right]^{-1} dr \otimes dr - r^2 \, g_{S^2} \,, \tag{1}$$

where the parameter $M \in \mathbb{R}_{>0}$ coincides with the ADM mass of the black hole geometry, and

$$g_{S^2} = d\theta \otimes d\theta + \sin^2(\theta) \, d\varphi \otimes d\varphi$$

is the metric on the unit 2-sphere. This representation of the Schwarzschild metric is defined for all $r \in \mathbb{R}_{>0}\backslash\{2M\}$ and features two types of singularities, namely a spacelike curvature singularity at $r = 0$ and a coordinate singularity at $r = 2M$, with the latter being the location of the event horizon $\mathfrak{M} \cap \partial J^-(\mathscr{I}^+)$, that is, the boundary of the causal past of future null infinity. The Schwarzschild black hole geometry may thus be separated into two connected components: the component $B_{\mathrm{I}} := \mathbb{R} \times \mathbb{R}_{>2M} \times S^2$, which is the domain of outer communication, and the component $B_{\mathrm{II}} := \mathbb{R} \times (0, 2M) \times S^2$, which is the future trapped region or black hole region $\mathfrak{M} \backslash J^-(\mathscr{I}^+) \neq \emptyset$. We remark that on B_{I}, the Schwarzschild time coordinate t is a Cauchy temporal function, i.e., it yields a foliation of this region by smooth, spacelike Cauchy hypersurfaces (see Sect. 2.3). However, due to the degeneracy of the Schwarzschild coordinates at—and the violation of the staticity of the Schwarzschild metric across—the event horizon, the level sets of t do not foliate the Schwarzschild black hole geometry.

We next recall the usual derivation of compactified Kruskal–Szekeres coordinates, which we restrict, for the purposes of the present work, to the region $B_{\mathrm{I}} \cup B_{\mathrm{II}}$. These coordinates are regular for all values of $r \in \mathbb{R}_{>0}$, locate the event horizon at finite coordinate values, and result in a compactification of the spacetime required for the construction of Penrose diagrams. We begin by transforming the Schwarzschild coordinates into Eddington–Finkelstein double-null coordinates [13, 15]

$$\mathfrak{T}^{\mathrm{EF}} : \begin{cases} \mathbb{R} \times \mathbb{R}_{>0} \times (0, \pi) \times [0, 2\pi) \to \mathbb{R} \times \mathbb{R} \times (0, \pi) \times [0, 2\pi) \\ (t, r, \theta, \varphi) \mapsto (u, v, \theta, \varphi) \end{cases}$$

with

$$\begin{cases} u = t - r_\star \quad \text{and} \quad v = t + r_\star \quad \text{for } B_{\mathrm{I}} \\ u = t + r_\star \quad \text{and} \quad v = -t + r_\star \quad \text{for } B_{\mathrm{II}} \,, \end{cases}$$

where

$$r_\star := r + 2M \ln \left| \frac{r}{2M} - 1 \right| \in \begin{cases} \mathbb{R} & \text{for } B_{\mathrm{I}} \\ \mathbb{R}_{<0} & \text{for } B_{\mathrm{II}} \end{cases}$$

is the Regge–Wheeler coordinate, and $v - u \in \mathbb{R}$ for B_{I} as well as $v + u \in \mathbb{R}_{<0}$ for B_{II}. The Schwarzschild metric in Eddington–Finkelstein double-null coordinates reads

$$g = \frac{1}{2} \left| 1 - \frac{2M}{r} \right| (du \otimes dv + dv \otimes du) - r^2 \, g_{S^2} \,.$$

We then apply the transformation into the Kruskal–Szekeres double-null coordinate system

$$\mathfrak{T}^{\mathrm{KS1}} : \begin{cases} \mathbb{R} \times \mathbb{R} \times (0, \pi) \times [0, 2\pi) \rightarrow \left(-\dfrac{\pi}{2}, \dfrac{\pi}{2}\right) \times \left(0, \dfrac{\pi}{2}\right) \times (0, \pi) \times [0, 2\pi) \\ \qquad\qquad (u, v, \theta, \varphi) \mapsto (U, V, \theta, \varphi) \end{cases}$$

with

$$\begin{cases} \tan(U) = -e^{-u/(4M)} \text{ and } \tan(V) = e^{v/(4M)} \text{ for } \mathrm{B_I} \\ \tan(U) = e^{u/(4M)} \quad\text{ and } \tan(V) = e^{v/(4M)} \text{ for } \mathrm{B_{II}}, \end{cases}$$

where $\tan(U)\tan(V) \in \mathbb{R}_{<0}$ for $\mathrm{B_I}$ and $\tan(U)\tan(V) \in (0, 1)$ for $\mathrm{B_{II}}$. Finally, we transform the Kruskal–Szekeres double-null coordinates into a compactified form of the usual Kruskal–Szekeres spacetime coordinates [23, 39]

$$\mathfrak{T}^{\mathrm{KS2}} : \begin{cases} \left(-\dfrac{\pi}{2}, \dfrac{\pi}{2}\right) \times \left(0, \dfrac{\pi}{2}\right) \times (0, \pi) \times [0, 2\pi) \rightarrow \left(-\dfrac{\pi}{4}, \dfrac{\pi}{4}\right) \times \left(-\dfrac{\pi}{4}, \dfrac{\pi}{2}\right) \\ \qquad\qquad\qquad\qquad\qquad\qquad\qquad\qquad\qquad \times (0, \pi) \times [0, 2\pi) \\ \qquad\qquad (U, V, \theta, \varphi) \mapsto (T, X, \theta, \varphi) \end{cases}$$

with

$$T = \frac{U + V}{2} \quad\text{and}\quad X = \frac{-U + V}{2} \quad\text{for } \mathrm{B_I} \cup \mathrm{B_{II}},$$

where $T \in (|X - \pi/4| - \pi/4, -|X - \pi/4| + \pi/4)$ and $X \in (0, \pi/2)$ for $\mathrm{B_I}$ and $T \in (|X|, \pi/4)$ and $X \in (-\pi/4, \pi/4)$ for $\mathrm{B_{II}}$. Using these coordinates, the Schwarzschild metric can be represented as

$$\boldsymbol{g} = \frac{32M^3\, e^{-r/(2M)}}{\cos^2(U)\cos^2(V)\, r}\, (\mathrm{d}T \otimes \mathrm{d}T - \mathrm{d}X \otimes \mathrm{d}X) - r^2\, \boldsymbol{g}_{S^2}.$$

We note in passing that the Kruskal–Szekeres time coordinate T is a temporal function on $\mathrm{B_I} \cup \mathrm{B_{II}}$ (cf. Definition 2.2 in Sect. 2.3). Furthermore, even though Kruskal–Szekeres spacetime coordinates are more general than required, they are—and yield representations of geometric quantities that are—nevertheless still fairly simple and easy to handle. However, if desired, one may as well work with different types of compactified horizon-penetrating coordinate systems derived from, e.g., Gullstrand–Painlevé coordinates, Lemaître coordinates, or advanced Eddington–Finkelstein coordinates [20, 24, 29].

2.2 Penrose diagram of the Schwarzschild black hole geometry

Due to the particular product structure of the Schwarzschild metric, that is,

$$\boldsymbol{g} = \boldsymbol{g}_{\mathrm{L}}^{(2)} \oplus \boldsymbol{g}_{\mathrm{R}}^{(2)} \quad\text{on}\quad \mathfrak{M} = \mathfrak{M}_{\mathrm{L}}^{(2)} \times \mathfrak{M}_{\mathrm{R}}^{(2)} \tag{2}$$

Table 1 Relations between Schwarzschild and Kruskal–Szekeres asymptotics

	$r \to \infty$	$r \to 2M$	$r \to 0$	$t \to \pm\infty$
B_I	$T = \pm[X - \pi/2]$	$T = \pm X$		$T = \mp[X - \pi/2], \ \ T = \pm X$
B_{II}		$T = \pm X$	$T = \pi/4$	$T = \mp X$

with

$$g(Y_L + Y_R, Z_L + Z_R) = g_L^{(2)}(Y_L, Z_L) + g_R^{(2)}(Y_R, Z_R)$$

for $Y_k, Z_k \in \Gamma\left(T\mathfrak{M}_k^{(2)}\right)$, $k \in \{L, R\}$, and the identification

$$T\left(\mathfrak{M}_L^{(2)} \times \mathfrak{M}_R^{(2)}\right) = T\mathfrak{M}_L^{(2)} \oplus T\mathfrak{M}_R^{(2)} \, ,$$

where $g_L^{(2)}$ and $g_R^{(2)}$ are 2-dimensional Lorentzian and Riemannian metrics on

$$\mathfrak{M}_L^{(2)} \cong \mathfrak{M}\backslash SO(3) \cong \mathbb{R}^2 \quad \text{and} \quad \mathfrak{M}_R^{(2)} \cong S^2 \, ,$$

respectively, any causal vector with respect to g is also a causal vector with respect to $g_L^{(2)}$ [9, 42]. This makes it possible to analyze the causal relations between different points in—and thus understanding the global causal structure of—the Schwarzschild black hole geometry using a Penrose diagram, where the metric $g_L^{(2)}$ on this diagram is locally as well as conformally equivalent to the actual metric g with every point corresponding to a 2-sphere. For the construction of this Penrose diagram, we employ the relations

$$\begin{cases} \dfrac{\sin(2T)}{\sin(2X)} = \tanh\left(t/(4M)\right) & \text{and} \quad \dfrac{\cos(2T)}{\cos(2X)} = -\coth\left(r_\star/(4M)\right) & \text{for } B_I \\[2ex] \dfrac{\sin(2T)}{\sin(2X)} = -\coth\left(t/(4M)\right) & \text{and} \quad \dfrac{\cos(2T)}{\cos(2X)} = -\tanh\left(r_\star/(4M)\right) & \text{for } B_{II} \end{cases}$$

between the Schwarzschild and the compactified Kruskal–Szekeres spacetime coordinates, which lead to the asymptotics shown in Table 1. These asymptotics may be used to define the relevant structures of the Penrose diagram, namely future/past timelike infinity $i^\pm = (T = \pm\pi/4, X = \pi/4)$, future/past null infinity $\mathscr{I}^\pm = \{(T, X) \,|\, T = \pm(-X + \pi/2)$ and $\pi/4 < X < \pi/2\}$, spacelike infinity $i^0 = (T = 0, X = \pi/2)$, the event horizon at $\{(T, X) \,|\, T = X$ and $0 \le X \le \pi/4\}$, and the location of the curvature singularity at $\{(T, X) \,|\, T = \pi/4$ and $-\pi/4 \le X \le \pi/4\}$. We depict the Penrose diagram of the Schwarzschild black hole geometry $B_I \cup B_{II}$ in Fig. 1.

2.3 Cauchy surfaces and time-type functions

We now recall the concepts of Cauchy surfaces and time-type functions.

Definition 2.1 *A Cauchy surface of a connected, time-orientable Lorentzian manifold* $(\mathfrak{M}, g)$ *is any subset* $\mathfrak{N} \subset \mathfrak{M}$ *that is closed and achronal, and has the domain of*

Fig. 1 Penrose diagram of the exterior and interior regions of the Schwarzschild black hole geometry
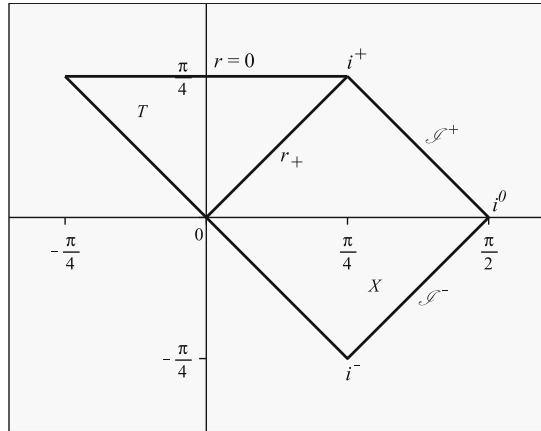
dependence $D(\mathfrak{N}) = \mathfrak{M}$, *i.e., it is intersected by every inextensible timelike curve exactly once.*

A Cauchy surface is therefore a topological hypersurface [28], which can be approximated by a smooth, spacelike hypersurface [3]. Moreover, if $(\mathfrak{M}, \boldsymbol{g})$ admits a Cauchy surface, it is globally hyperbolic [17].

Definition 2.2 *We let* $(\mathfrak{M}, \boldsymbol{g})$ *be a connected, time-orientable Lorentzian manifold. A function* $\mathfrak{t}: \mathfrak{M} \to \mathbb{R}$ *is called a*

1. *generalized time function if it is strictly increasing on any future-directed causal curve.*
2. *time function if it is a continuous generalized time function.*
3. *temporal function if it is a smooth function with future-directed, timelike gradient* $\nabla \mathfrak{t} = g^{\mathfrak{t}\nu}\partial_\nu$.

According to [2, 16], there is the following relation between time-type functions and the notion of global hyperbolicity.

Proposition 2.3 *Any connected, time-orientable, globally hyperbolic Lorentzian manifold* $(\mathfrak{M}, \boldsymbol{g})$ *contains a Cauchy temporal function* $\mathfrak{t}$, *that is, a temporal function for which the level sets* $\mathfrak{t}^{-1}(\,.\,)$ *are smooth, spacelike Cauchy hypersurfaces* $(\mathfrak{N}_\mathfrak{t})_{\mathfrak{t}\in\mathbb{R}}$ *with* $\mathfrak{N}_\mathfrak{t} := \{\mathfrak{t}\} \times \mathfrak{N}$ *and* $\mathfrak{N}_\mathfrak{t} \subset J^-(\mathfrak{N}_{\mathfrak{t}'})$ *for all* $\mathfrak{t} < \mathfrak{t}'$.

We remark that a coordinate system $(\mathfrak{t}, \boldsymbol{x})$ on $\mathfrak{M}$, where $\mathfrak{t} \in \mathbb{R}$ is a Cauchy temporal function and $\boldsymbol{x}$ are coordinates on $\mathfrak{N}$, may be understood as corresponding to an observer who is co-moving along the flow lines of the Killing field $\Gamma(T\mathfrak{M}) \ni \boldsymbol{K} = \partial_\mathfrak{t}$.

3 Geometric construction procedure of horizon-penetrating Cauchy coordinates for the Schwarzschild black hole geometry

We begin by simplifying the geometric shape of the Penrose diagram of the Schwarzschild black hole geometry $B_I \cup B_{II}$ transforming the trapezoid shown in

Fig. 2a into a centrally symmetric diamond as in Fig. 2f. In more detail, we first rotate the trapezoid counter-clockwise about an angle of $\pi/4$ rad (Fig. 2a $\rightarrow$ Fig. 2b) employing the transformation

$$\mathfrak{T}^{(1)} : \begin{cases} \left(-\dfrac{\pi}{4}, \dfrac{\pi}{4}\right) \times \left(-\dfrac{\pi}{4}, \dfrac{\pi}{2}\right) \rightarrow \left(0, \dfrac{\pi}{2\sqrt{2}}\right) \times \left(-\dfrac{\pi}{2\sqrt{2}}, \dfrac{\pi}{2\sqrt{2}}\right) \\ (T = T^{(0)}, X = X^{(0)}) \mapsto (T^{(1)}, X^{(1)}) \end{cases} \tag{3}$$

with

$$T^{(1)} = \frac{T^{(0)} + X^{(0)}}{\sqrt{2}} \quad \text{and} \quad X^{(1)} = \frac{-T^{(0)} + X^{(0)}}{\sqrt{2}} \, ,$$

where $T^{(1)} < X^{(1)} + \pi/(2\sqrt{2})$ for $-\pi/(2\sqrt{2}) < X^{(1)} \leq 0$. We then deform the resulting trapezoid into a rectangle (Fig. 2b $\rightarrow$ Fig. 2c) by identifying the line

$$\left\{ (T^{(1)}, X^{(1)}) \, \middle| \, T^{(1)} = X^{(1)} + \pi/(2\sqrt{2}) \text{ and } -\pi/(2\sqrt{2}) \leq X^{(1)} \leq 0 \right\}$$

with the line

$$\left\{ (T^{(1)}, X^{(1)}) \, \middle| \, 0 \leq T^{(1)} \leq \pi/(2\sqrt{2}) \text{ and } X^{(1)} = -\pi/(2\sqrt{2}) \right\}$$

applying the transformation

$$\mathfrak{T}^{(2)} : \begin{cases} \left(0, \dfrac{\pi}{2\sqrt{2}}\right) \times \left(-\dfrac{\pi}{2\sqrt{2}}, \dfrac{\pi}{2\sqrt{2}}\right) \rightarrow \left(0, \dfrac{\pi}{2\sqrt{2}}\right) \times \left(-\dfrac{\pi}{2\sqrt{2}}, \dfrac{\pi}{2\sqrt{2}}\right) \\ (T^{(1)}, X^{(1)}) \mapsto (T^{(2)}, X^{(2)}) \end{cases} \tag{4}$$

with

$$T^{(2)} = T^{(1)} \quad \text{and} \quad X^{(2)} = \frac{T^{(1)}/2 - X^{(1)}}{T^{(1)}\sqrt{2}/\pi - 1} \, .$$

Subsequently, we translate the rectangle by the distance $-\pi/(4\sqrt{2})$ along the ordinate (Fig. 2c $\rightarrow$ Fig. 2d) and rotate it clockwise about an angle of $\arctan(1/2)$ rad (Fig. 2d $\rightarrow$ Fig. 2e) using the mappings

$$\mathfrak{T}^{(3)} : \begin{cases} \left(0, \dfrac{\pi}{2\sqrt{2}}\right) \times \left(-\dfrac{\pi}{2\sqrt{2}}, \dfrac{\pi}{2\sqrt{2}}\right) \rightarrow \left(-\dfrac{\pi}{4\sqrt{2}}, \dfrac{\pi}{4\sqrt{2}}\right) \times \left(-\dfrac{\pi}{2\sqrt{2}}, \dfrac{\pi}{2\sqrt{2}}\right) \\ (T^{(2)}, X^{(2)}) \mapsto (T^{(3)}, X^{(3)}) \end{cases} \tag{5}$$

with

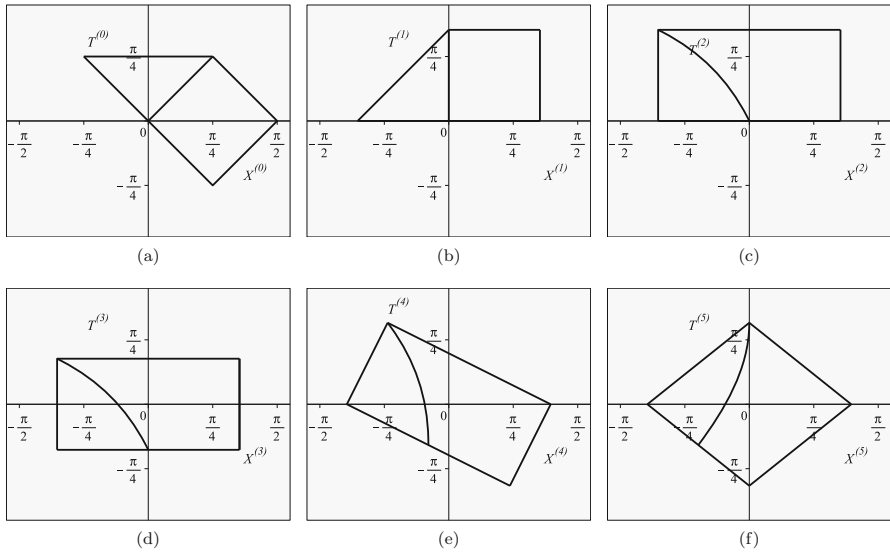$$T^{(3)} = T^{(2)} - \frac{\pi}{4\sqrt{2}} \quad \text{and} \quad X^{(3)} = X^{(2)}$$

Fig. 2 Geometric representations of the transformations (3)–(7)

as well as

$$\mathfrak{T}^{(4)} : \begin{cases} \left(-\dfrac{\pi}{4\sqrt{2}}, \dfrac{\pi}{4\sqrt{2}}\right) \times \left(-\dfrac{\pi}{2\sqrt{2}}, \dfrac{\pi}{2\sqrt{2}}\right) \rightarrow \left(-\dfrac{\pi}{\sqrt{10}}, \dfrac{\pi}{\sqrt{10}}\right) \times \left(-\sqrt{\dfrac{5}{2}}\dfrac{\pi}{4}, \sqrt{\dfrac{5}{2}}\dfrac{\pi}{4}\right) \\ \qquad\qquad\qquad (T^{(3)}, X^{(3)}) \mapsto (T^{(4)}, X^{(4)}) \end{cases} \tag{6}$$

with

$$T^{(4)} = \frac{2T^{(3)} - X^{(3)}}{\sqrt{5}} \quad \text{and} \quad X^{(4)} = \frac{T^{(3)} + 2X^{(3)}}{\sqrt{5}},$$

where

$$T^{(4)} < \Theta\left(X^{(4)} + \sqrt{\frac{5}{2}}\frac{\pi}{4}\right)\Theta\left(-\frac{3\pi}{4\sqrt{10}} - X^{(4)}\right)\left[2X^{(4)} + \sqrt{\frac{5}{2}}\frac{\pi}{2}\right]$$

$$+ \Theta\left(X^{(4)} + \frac{3\pi}{4\sqrt{10}}\right)\Theta\left(\sqrt{\frac{5}{2}}\frac{\pi}{4} - X^{(4)}\right)\frac{1}{2}\left[-X^{(4)} + \sqrt{\frac{5}{2}}\frac{\pi}{4}\right]$$

and

$$- \Theta\left(X^{(4)} + \sqrt{\frac{5}{2}}\frac{\pi}{4}\right)\Theta\left(\frac{3\pi}{4\sqrt{10}} - X^{(4)}\right)\frac{1}{2}\left[X^{(4)} + \sqrt{\frac{5}{2}}\frac{\pi}{4}\right]$$

$$+ \Theta\left(X^{(4)} - \frac{3\pi}{4\sqrt{10}}\right)\Theta\left(\sqrt{\frac{5}{2}}\frac{\pi}{4} - X^{(4)}\right)\left[2X^{(4)} - \sqrt{\frac{5}{2}}\frac{\pi}{2}\right] < T^{(4)}.$$

Here, $\Theta(\,.\,) := [1 + \mathrm{sgn}(\,.\,)]/2$ is the Heaviside step function. Lastly, we employ the shear transformation

$$
\mathfrak{T}^{(5)} : \left\{
\begin{array}{c}
\left(-\dfrac{\pi}{\sqrt{10}}, \dfrac{\pi}{\sqrt{10}}\right) \times \left(-\sqrt{\dfrac{5}{2}}\dfrac{\pi}{4}, \sqrt{\dfrac{5}{2}}\dfrac{\pi}{4}\right) \rightarrow \left(-\dfrac{\pi}{\sqrt{10}}, \dfrac{\pi}{\sqrt{10}}\right) \times \left(-\sqrt{\dfrac{5}{2}}\dfrac{\pi}{4}, \sqrt{\dfrac{5}{2}}\dfrac{\pi}{4}\right) \\[6pt]
(T^{(4)}, X^{(4)}) \mapsto (T^{(5)}, X^{(5)})
\end{array}
\right.
\tag{7}
$$

with

$$
V = T^{(5)} = T^{(4)} \quad \text{and} \quad W = X^{(5)} = \frac{3T^{(4)}}{4} + X^{(4)},
$$

where $4|X^{(5)}|/5 - \pi/\sqrt{10} < T^{(5)} < -4|X^{(5)}|/5 + \pi/\sqrt{10}$, in order to obtain the centrally symmetric diamond (Fig. 2e → Fig. 2f). The composition of the transformations (3)–(7) yields the relations

$$
\begin{aligned}
V &= \frac{2}{\sqrt{10}\,[\pi - X - T]}\left(-(X+T)^2 + \pi\left[X + 2T - \frac{\pi}{4}\right]\right) \\[6pt]
W &= \frac{5}{2\sqrt{10}\,[\pi - X - T]}\left(-(X+T)^2 + \frac{\pi}{2}\left[3X + T - \frac{\pi}{2}\right]\right).
\end{aligned}
\tag{8}
$$

Next, we formulate conditions for the determination of specific indexed families of smooth functions $(V_\lambda(W)\,|\,\lambda \in \mathbb{R})$ that foliate the diamond:

(C1) Limit conditions: $V_{\pm\infty}(W) = \pm\dfrac{4}{5}\big[-|W| + \mu\big]$

(C2) Boundary conditions: $V_\lambda(\pm\mu) = 0 \quad \forall \lambda \in \mathbb{R}$

(C3) Smoothness condition: $V_{|\lambda|<\infty}(W) \in C^\infty\big((-\mu, \mu), \mathbb{R}\big)$

(C4) Causality conditions: $-\dfrac{4}{5} < \partial_W V_\lambda < \dfrac{8}{5}\dfrac{4W - \pi\sqrt{10}}{10V_\lambda - \pi\sqrt{10}}$

$$\text{and} \quad 0 < \partial_\lambda V_\lambda \forall\, W \in (-\mu, \mu)$$

(C5) Symmetry condition: $\lambda \mapsto -\lambda \iff (V_\lambda, W) \mapsto (-V_\lambda, W)$,

where $\mu := \sqrt{5/2}\,\pi/4$. We note that the limit conditions in (C1) define the geometrical shape of the diamond, while the boundary conditions in (C2) specify the starting point and the endpoint of the functions V_λ. Besides, the first boundary condition $(V_\lambda, W) = (0, +\mu)$ gives rise to asymptotic flatness at spacelike infinity, whereas the second boundary condition $(V_\lambda, W) = (0, -\mu)$ ensures that the functions hit the curvature singularity only asymptotically. The meaning of the smoothness condition in (C3) is obvious. Moreover, the causality conditions in (C4) constrain the functions to be spacelike on the one hand, and nonintersecting on the other. Direct computations show that these conditions imply that the gradient $\nabla\lambda$ on $B_I \cup B_{II}$ is future-directed and timelike, and hence that λ is a temporal function. The reflection symmetry provided by the symmetry condition in (C5), however, is only incorporated for convenience. Therefore, it is not strictly required and may be dropped if desired. Finally, we consider the indices λ of such families as the time variables of new global coordinate systems on $B_I \cup B_{II}$ defined via the general transformation

$$\mathfrak{T}^C : \begin{cases} \left(-\dfrac{\pi}{4}, \dfrac{\pi}{4}\right) \times \left(-\dfrac{\pi}{4}, \dfrac{\pi}{2}\right) \times (0, \pi) \times [0, 2\pi) \to \mathbb{R} \times \left(-\dfrac{\pi}{4}, \dfrac{\pi}{2}\right) \\ \qquad\qquad\qquad\qquad\qquad\qquad\qquad\qquad \times (0, \pi) \times [0, 2\pi) \\ \qquad\qquad\qquad (T, X, \theta, \varphi) \mapsto (\lambda, X', \theta, \varphi) \end{cases}$$

with

$$\lambda = \lambda(T, X) \quad \text{and} \quad X' = X.$$

We now prove that the level sets of the time variables λ, which are by the above construction smooth, spacelike, nonintersecting, asymptotically flat, and foliate the entire Schwarzschild black hole geometry, constitute Cauchy hypersurfaces.

Proposition 3.1 *We let $\mathfrak{S} \equiv \mathfrak{S}_{\lambda_0}$ be homeomorphic to the subset*

$$\{\lambda_0\} \times \left(-\frac{\pi}{4}, \frac{\pi}{2}\right) \times S^2 \subset B_I \cup B_{II}$$

of the joined exterior and interior regions of the Schwarzschild black hole geometry, where this subset is a level set of the time coordinates λ at $\lambda_0 = $ const. Then, $\mathfrak{S}$ is a Cauchy hypersurface.

Proof We begin by noting that $\mathfrak{S}$ is closed in $B_I \cup B_{II}$, which is an immediate consequence of the fact that its complement

$$\mathfrak{S}^c \cong \mathbb{R} \backslash \{\lambda_0\} \times \left(-\frac{\pi}{4}, \frac{\pi}{2}\right) \times S^2$$

is open. Moreover, as the time coordinates λ are temporal functions on $B_I \cup B_{II}$, that is, $B_I \cup B_{II}$ is stably causal [26], any connected causal curve through this region can intersect $\mathfrak{S}$ at most once. Thus, $\mathfrak{S}$ is achronal. It remains to be shown that the domain of dependence $D(\mathfrak{S}) = B_I \cup B_{II}$. To this end, it suffices to demonstrate that the total Cauchy horizon $H(\mathfrak{S})$ of $\mathfrak{S}$ is empty, using a proof by contradiction. Hence, we suppose that there exists a point p in the future Cauchy horizon $H^+(\mathfrak{S})$. Since $\mathfrak{S}$ is achronal and edgeless, p is the future endpoint of a null geodesic $\gamma \subset H^+(\mathfrak{S})$, which is past inextensible in $B_I \cup B_{II}$ [40]. From this, it follows that $\gamma \subset J^+(\mathfrak{S}) \cap J^-(p)$. Furthermore, as $B_I \cup B_{II}$ is globally hyperbolic, $J^+(\mathfrak{S}) \cap J^-(p)$ is contained in a compact set. And given that γ cannot be imprisoned in a compact set that is stably causal [25], we are led to a contradiction. Accordingly, $H^+(\mathfrak{S}) = \emptyset$. Due to time duality, we can argue that the same holds true for $H^-(\mathfrak{S})$, and therefore $H(\mathfrak{S}) = \emptyset$. $\qquad\square$

4 Application to an integrated algebraic sigmoid function

In this section, we study a simple example of the families $(V_\lambda(W) \,|\, \lambda \in \mathbb{R})$, which is based on an integrated algebraic sigmoid function. To be more precise, since our 2-dimensional diagrammatic representation of the Schwarzschild black hole geometry
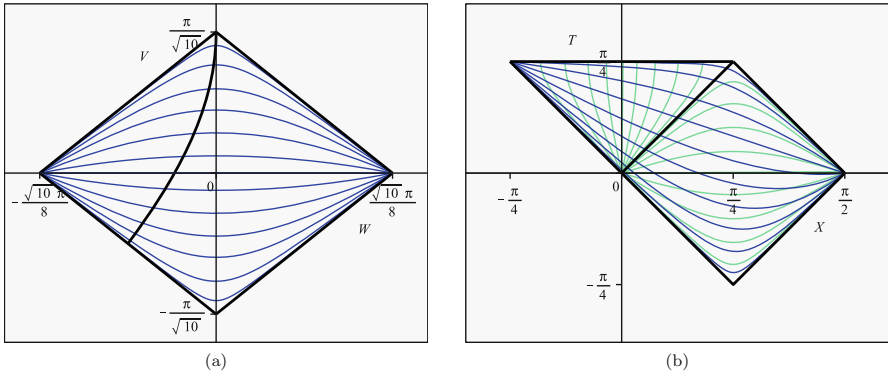
Fig. 3 Diamond representation of the Schwarzschild black hole geometry with smooth functions $V_\lambda(W)$ defined in (10) for index values $\lambda \in \pm\{0, 0.2, 0.5, 0.9, 1.5, 3, 8\}$ (**a**) and Penrose diagram of the Schwarzschild black hole geometry with level sets of the Cauchy temporal function λ specified in (11) for values in $\{-10, -3.2, -1.6, -0.9, -0.45, -0.1, 0.28, 0.8, 2.1, 6.5\}$ (blue curves) and with level sets of the normalized Schwarzschild time coordinate $t/M \in \pm\{0, 1.24, 2.77, 4.75, 7.78\}$ for B_I and $t/M \in \pm\{0, 0.86, 1.96, 3.58, 6.09\}$ for B_{II} (aquamarine curves) for comparison (**b**)

$B_I \cup B_{II}$ is in the form of a centrally symmetric diamond, we are interested in a smooth approximation of the absolute value function $|W|$ (see the limit conditions in ($\mathcal{C}1$)). By considering the derivative of the absolute value function, namely the signum function $\mathrm{sgn}(W)$, we may easily find such a smooth approximation in terms of the integral of a hyperbolic tangent, an arctangent function, or an algebraic function. In the following, we work out the horizon-penetrating Cauchy coordinate system and the metric representation associated with the algebraic sigmoid function approximation

$$\mathrm{sgn}(W) \approx \frac{|\lambda|W}{\sqrt{1 + \lambda^2 W^2}}, \tag{9}$$

where λ serves as approximation parameter, because this example can be treated completely analytically. Thus, integrating (9) and imposing the conditions defined in ($\mathcal{C}1$)–($\mathcal{C}5$), we obtain

$$V_\lambda(W) = \frac{4}{5\lambda}\left[\sqrt{1 + \lambda^2\mu^2} - \sqrt{1 + \lambda^2 W^2}\right] \tag{10}$$

(for an illustration, see Fig. 3a). Inverting this expression with respect to λ and substituting the relations specified in (8) gives rise to the transformation from compactified Kruskal–Szekeres spacetime coordinates into the horizon-penetrating Cauchy coordinates

$$\mathfrak{T}^C : \begin{cases} \left(-\dfrac{\pi}{4}, \dfrac{\pi}{4}\right) \times \left(-\dfrac{\pi}{4}, \dfrac{\pi}{2}\right) \times (0, \pi) \times [0, 2\pi) \to \mathbb{R} \\ \qquad \times \left(-\dfrac{\pi}{4}, \dfrac{\pi}{2}\right) \times (0, \pi) \times [0, 2\pi) \\ \qquad (T, X, \theta, \varphi) \mapsto (\lambda, X', \theta, \varphi) \end{cases}$$

with

$$\lambda = \frac{5V(T,X)}{2\sqrt{\left[W(T,X)^2 - \dfrac{25V(T,X)^2}{16} + \dfrac{5\pi^2}{32}\right]^2 - \dfrac{5\pi^2 W(T,X)^2}{8}}} \quad \text{and} \quad X' = X.$$

(11)

The Schwarzschild metric formulated via these coordinates reads

$$\begin{aligned}
\boldsymbol{g} = {}& \frac{32M^3\, e^{-r/(2M)}}{[15\pi\lambda + \sqrt{160 + 25\pi^2\lambda^2}\,]^4 \cos^2(U)\cos^2(V)\, r} \Big[400\pi^2\, \mathscr{C}_\lambda^2\, \mathrm{d}\lambda \otimes \mathrm{d}\lambda - 40\pi\, \mathscr{C}_\lambda \mathscr{C}_{X'} \\
& \times (\mathrm{d}\lambda \otimes \mathrm{d}X' + \mathrm{d}X' \otimes \mathrm{d}\lambda) + \big(4\mathscr{C}_{X'}^2 - [15\pi\lambda + \sqrt{160 + 25\pi^2\lambda^2}\,]^4\big)\, \mathrm{d}X' \otimes \mathrm{d}X'\Big] - r^2\, \boldsymbol{g}_{S^2},
\end{aligned}$$

where

$$\begin{aligned}
\mathscr{C}_\lambda := {}& \frac{20\,[4X' - 5\pi]}{\sqrt{160 + 25\pi^2\lambda^2}} \\
& - \frac{\sqrt{5\pi}}{\sqrt{5\pi\lambda^2\,[X' - \pi/4]^2 - 2\,[4X' - 3\pi]}} \left[\frac{10\lambda\,(8X'^2 - 2\pi X' - \pi^2)}{\sqrt{160 + 25\pi^2\lambda^2}} + 3\,(4X' - 3\pi)\right] \\
\mathscr{C}_{X'} := {}& 10\,\big[5\pi^2\lambda^2 + \pi\lambda\sqrt{160 + 25\pi^2\lambda^2} + 8\big] \\
& + \frac{\sqrt{5\pi}\,\big(15\pi\lambda + \sqrt{160 + 25\pi^2\lambda^2}\,\big)\big(5\pi\lambda^2\,[X' - \pi/4] - 4\big)}{\sqrt{5\pi\lambda^2\,[X' - \pi/4]^2 - 2\,[4X' - 3\pi]}}.
\end{aligned}$$

We depict the foliation of the Schwarzschild black hole geometry by the level sets of λ in the Penrose diagram in Fig. 3b.

5 Generalization to the Reissner–Nordström black hole geometry

We generalize our results to the Reissner–Nordström black hole geometry up to the Cauchy horizon. This spacetime is, like the Schwarzschild black hole geometry, a connected, smooth, globally hyperbolic and asymptotically flat Lorentzian 4-manifold $(\mathfrak{M}, \boldsymbol{g})$ with $\mathfrak{M}$ being homeomorphic to $\mathbb{R}^2 \times S^2$. It is, however, based on the unique 2-parameter family of exact, spherically symmetric solutions $\boldsymbol{g}$ of the more general Einstein–Maxwell equations, which can be used to analyze the final equilibrium state of the dynamical evolution of the gravitational field of an isolated, electrically charged, spherically symmetric black hole. We begin by performing the replacement

$$1 - \frac{2M}{r} \;\rightarrow\; 1 - \frac{2M}{r} + \frac{Q^2}{r^2} =: \frac{\Delta(r)}{r^2}$$

in the g_{tt} and g_{rr} components of the Schwarzschild metric (1), where the parameter $Q \in \mathbb{R}$ denotes the electrical charge of the black hole geometry satisfying the relation $0 < |Q| < M$, and the two real-valued roots $r_\pm := M \pm \sqrt{M^2 - Q^2}$ of the function $\Delta: \mathbb{R}_{>0} \to [-M^2 + Q^2, \infty)$ define an outer and an inner event horizon, respectively. This

replacement gives rise to the Schwarzschild-type representation of the nonextreme Reissner–Nordström metric [27, 32]

$$\boldsymbol{g} = \frac{\Delta}{r^2}\, dt \otimes dt - \frac{r^2}{\Delta}\, dr \otimes dr - r^2\, \boldsymbol{g}_{S^2}\,. \tag{12}$$

We point out that the canonical Reissner–Nordström black hole geometry comprises the three connected components $B_I := \mathbb{R} \times \mathbb{R}_{>r_+} \times S^2$, $B_{II} := \mathbb{R} \times (r_-, r_+) \times S^2$, and $B_{III} := \mathbb{R} \times (0, r_-) \times S^2$, which have a causal structure that is qualitatively different from the one of the Schwarzschild case, as B_{III} contains a curvature singularity at $r = 0$ with timelike character and, more importantly for the present purpose, the inner event horizon at $r = r_-$ is a Cauchy horizon. Consequently, since our geometric construction procedure requires the underlying Lorentzian manifold to be globally hyperbolic, we consider only the region $B_I \cup B_{II}$ of the Reissner–Nordström black hole geometry up to the Cauchy horizon. We then transform the Schwarzschild-type coordinates into compactified Kruskal–Szekeres-type coordinates

$$\mathfrak{X}^{KS} : \begin{cases} \mathbb{R} \times \mathbb{R}_{>0} \times (0, \pi) \times [0, 2\pi) \to \left(-\dfrac{\pi}{4}, \dfrac{\pi}{2}\right) \\ \qquad\qquad \times \left(-\dfrac{\pi}{4}, \dfrac{\pi}{2}\right) \times (0, \pi) \times [0, 2\pi) \\ (t, r, \theta, \varphi) \mapsto (T, X, \theta, \varphi) \end{cases}$$

with

$$\begin{cases} T = \dfrac{1}{2}\arctan\left(\dfrac{\sinh(\alpha t)}{\cosh(\alpha r_\star)}\right) & \text{and} \quad X = -\dfrac{1}{2}\arctan\left(\dfrac{\cosh(\alpha t)}{\sinh(\alpha r_\star)}\right) + \dfrac{\pi\Theta(r_\star)}{2} & \text{for } B_I \\[2ex] T = -\dfrac{1}{2}\arctan\left(\dfrac{\cosh(\alpha t)}{\sinh(\alpha r_\star)}\right) + \dfrac{\pi\Theta(r_\star)}{2} & \text{and} \quad X = -\dfrac{1}{2}\arctan\left(\dfrac{\sinh(\alpha t)}{\cosh(\alpha r_\star)}\right) & \text{for } B_{II}\,, \end{cases}$$

where $T \in (|X - \pi/4| - \pi/4, -|X - \pi/4| + \pi/4)$ and $X \in (0, \pi/2)$ for B_I and $T \in (|X|, \pi/2 - |X|)$ and $X \in (-\pi/4, \pi/4)$ for B_{II}. Here, the Regge–Wheeler coordinate is defined as

$$r_\star := r + \frac{r_+^2}{r_+ - r_-}\, \ln\left|\frac{r}{r_+} - 1\right| - \frac{r_-^2}{r_+ - r_-}\, \ln\left(\frac{r}{r_-} - 1\right)$$

and $\alpha := (r_+ - r_-)/(2r_+^2)$ is a positive constant. The Reissner–Nordström metric (12) written in terms of these coordinates takes the form

$$\boldsymbol{g} = \frac{r_+ r_- \left(\frac{r}{r_-} - 1\right)^{1 - r_-^2/r_+^2} e^{-2\alpha r}}{\alpha^2 \cos^2(U) \cos^2(V)\, r^2}\, (dT \otimes dT - dX \otimes dX) - r^2\, \boldsymbol{g}_{S^2}\,.$$

Next, we employ the method introduced in Sect. 3 and work out the details of the analog of the specific integrated algebraic sigmoid function application (10) within
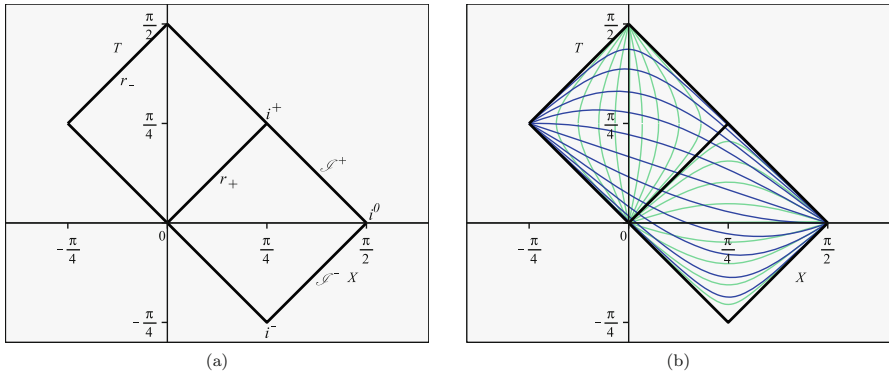
Fig. 4 Penrose diagram of the Reissner–Nordström black hole geometry up to the Cauchy horizon (**a**) and the same Penrose diagram with level sets of the Cauchy temporal function λ defined in (13) for values in $\pm\{0, 0.3, 0.65, 1.1, 2, 4\}$ (blue curves) and with level sets of the normalized Schwarzschild-type time coordinate $t/M \in \pm\{0, 1.24, 2.77, 4.75, 7.78\}$ for B_I and $t/M \in \pm\{0, 0.86, 1.96, 3.58, 6.09\}$ for B_{II} (aquamarine curves) for comparison (**b**)

the present framework. To this end, we have to perform the same steps as before, however, we may now omit transformation (4), because the Penrose diagram of the region $B_I \cup B_{II}$ of the Reissner–Nordström black hole geometry is already rectangularly shaped (cf. Fig. 4a). This in turn leads to the first causality condition in ($\mathcal{C}$4) assuming the form $|\partial_W V_\lambda| < 4/5$. Accordingly, we obtain the transformation from the above compactified Kruskal–Szekeres-type coordinates into the horizon-penetrating Cauchy coordinates

$$\mathfrak{T}^C : \begin{cases} \left(-\dfrac{\pi}{4}, \dfrac{\pi}{2}\right) \times \left(-\dfrac{\pi}{4}, \dfrac{\pi}{2}\right) \times (0, \pi) \times [0, 2\pi) \to \mathbb{R} \\ \qquad\qquad \times \left(-\dfrac{\pi}{4}, \dfrac{\pi}{2}\right) \times (0, \pi) \times [0, 2\pi) \\ (T, X, \theta, \varphi) \mapsto (\lambda, X', \theta, \varphi) \end{cases}$$

with

$$\lambda = \frac{6T + 2X - \pi}{\sqrt{10\left[(T-X)^2 - \dfrac{\pi^2}{4}\right]\left[T + X - \dfrac{\pi}{2}\right][T+X]}} \quad \text{and} \quad X' = X. \qquad (13)$$

Expressed via these coordinates, the Reissner–Nordström metric reads

$$\boldsymbol{g} = \frac{r_+ r_- (r/r_- - 1)^{1 - r_-^2/r_+^2} e^{-2\alpha r}}{\alpha^2 \cos^2(U) \cos^2(V) r^2} \bigg[\mathscr{G}^2 \mathrm{d}\lambda \otimes \mathrm{d}\lambda$$
$$+ \frac{\mathscr{E}\mathscr{G}}{\sqrt{1 + \mathscr{E}^2}} (\mathrm{d}\lambda \otimes \mathrm{d}X' + \mathrm{d}X' \otimes \mathrm{d}\lambda) - \frac{\mathrm{d}X' \otimes \mathrm{d}X'}{1 + \mathscr{E}^2} \bigg] - r^2 \, \boldsymbol{g}_{S^2} \, ,$$

where

$$\mathscr{E} := \frac{\sqrt{5}}{2} \left[\lambda \left(X' - \frac{\pi}{8} \right) + \sqrt{\frac{1}{10} + \frac{\pi^2 \lambda^2}{64}} \right]$$

and

$$\mathscr{G} := \frac{1}{10\lambda^2} \left[\left(\frac{1}{10} + \frac{\pi^2 \lambda^2}{64} \right) \left(1 + \mathscr{E}^2 \right) \right]^{-1/2} \left[3\sqrt{1 + \mathscr{E}^2} - \mathscr{E} - \sqrt{8 + \frac{5\pi^2 \lambda^2}{4}} \right].$$

We emphasize that the metric coefficients $g_{\lambda\lambda}$ and $g_{\lambda X'}$ are, despite their appearance, also regular at $\lambda = 0$, which can be directly seen from the limits

$$\lim_{|\lambda| \to 0} \mathscr{E} = \frac{1}{2\sqrt{2}} \quad \text{and} \quad \lim_{|\lambda| \to 0} \mathscr{G} = \frac{\sqrt{10}}{27} \left[4X'^2 - \pi X' - \frac{\pi^2}{2} \right] \in \left(-\sqrt{\frac{5}{2}} \frac{\pi^2}{24}, 0 \right).$$

Therefore, this metric representation is nondegenerate everywhere on $B_I \cup B_{II}$. Moreover, direct computations show that the gradient of the time coordinate λ defined in (13) is future-directed and timelike. And by using a proof similar to the one of the Schwarzschild case (see the end of Sect. 3), one can demonstrate that the level sets of this time coordinate are Cauchy hypersurfaces. Thus, λ is a Cauchy temporal function. The associated foliation of the region $B_I \cup B_{II}$ of the Reissner–Nordström black hole geometry is illustrated in the Penrose diagram in Fig. 4b. We note in passing that in the Schwarzschild limit $|Q| \to 0$, some of the level sets of λ lose their Cauchy property. This stems from the fact that all level sets located in the region above the line $3T = -X + \pi/2$ intersect the curvature singularity of the Schwarzschild trapezoid. Hence, one obtains only a foliation of the limiting spacetime by spacelike hypersurfaces.

6 Outlook

As a future research project, we plan on generalizing our method and results to the axially symmetric Kerr black hole geometry up to the Cauchy horizon, which involves two significant challenges. On the one hand, due to the existence of nonvanishing cross terms, the nonextreme Kerr metric does not have the particular product structure (2), making it impossible to directly locally relate the causal structure of the Kerr black hole geometry to that of the corresponding Penrose diagram similar to the cases of the spherically symmetric black hole geometries. On the other hand, the time variable of the usual Kruskal–Szekeres-type coordinate system for the nonextreme Kerr geometry [7, 34] is not a temporal function, which is in contrast to the Kruskal–Szekeres time variables of the Schwarzschild and nonextreme Reissner–Nordström geometries. Since this aspect is, however, paramount for the present method, we are required to first modify the construction of the analytic Kruskal–Szekeres-type extension of the nonextreme Kerr geometry accordingly. Otherwise, we could also work with a different horizon-penetrating coordinate system, which already features a time coordinate

that is a temporal function (for an example, see the coordinate system analyzed in, e.g., [33]), as the basis for our geometric approach altogether. While this may seem more suitable at first glance, the use of such a coordinate system could lead to yet unforeseen obstacles that would have to be resolved as well. In addition to this research project, we intend to apply our construction method to other spacetimes having the same metrical product structure as the Schwarzschild and Reissner–Nordström black hole geometries, thereby focusing on conceptual issues and the applicability of the method itself, as well as on the determination of the associated Cauchy coordinate systems.

References

1. Beig, R., Murchadha, N.Ó.: Late time behavior of the maximal slicing of the Schwarzschild black hole. Phys. Rev. D **57**, 4728 (1998)
2. Bernal, A.N., Sánchez, M.: Smoothness of time functions and the metric splitting of globally hyperbolic spacetimes. Commun. Math. Phys. **257**, 43 (2005)
3. Bernal, A.N., Sánchez, M.: Further results on the smoothability of Cauchy hypersurfaces and Cauchy time functions. Lett. Math. Phys. **77**, 183 (2006)
4. Brill, D.R., Cavallo, J.M., Isenberg, J.A.: K-surfaces in the Schwarzschild space-time and the construction of lattice cosmologies. J. Math. Phys. **21**, 2789 (1980)
5. Carter, B.: The complete analytic extension of the Reissner–Nordström metric in the special case $e^2 = m^2$. Phys. Lett. **21**, 423 (1966)
6. Carter, B.: Complete analytic extension of the symmetry axis of Kerr's solution of Einstein's equations. Phys. Rev. **141**, 1242 (1966)
7. Chandrasekhar, S.: The Mathematical Theory of Black Holes. Oxford University Press, New York (1983)
8. Choquet Bruhat, Y.: General Relativity and Einstein's Equations. Oxford University Press, New York (2009)
9. Chruściel, P.T.: Elements of General Relativity. Birkhäuser, Cham (2020)
10. Chruściel, P.T., Ölz, C.R., Szybka, S.J.: Space-time diagrammatics. Phys. Rev. D **86**, 124041 (2012)
11. Dennison, K.A., Baumgarte, T.W.: A simple family of analytical trumpet slices of the Schwarzschild spacetime. Class. Quantum Gravity **31**, 117001 (2014)
12. Eardley, D.M., Smarr, L.: Time functions in numerical relativity: marginally bound dust collapse. Phys. Rev. D **19**, 2239 (1979)
13. Eddington, A.S.: A comparison of Whitehead's and Einstein's formulae. Nature **113**, 192 (1924)

14. Estabrook, F., Wahlquist, H., Christensen, S., DeWitt, B., Smarr, L., Tsiang, E.: Maximally slicing a black hole. Phys. Rev. D **7**, 2814 (1973)
15. Finkelstein, D.: Past-future asymmetry of the gravitational field of a point particle. Phys. Rev. **110**, 965 (1958)
16. Geroch, R.: Spinor structure of space-times in general relativity. I. J. Math. Phys. **9**, 1739 (1968)
17. Geroch, R.: Domain of dependence. J. Math. Phys. **11**, 437 (1970)
18. Graves, J.C., Brill, D.R.: Oscillatory character of Reissner–Nordström metric for an ideal charged wormhole. Phys. Rev. **120**, 1507 (1960)
19. Griffiths, J.B., Podolský, J.: Exact Space-times in Einstein's General Relativity. Cambridge University Press, New York (2012)
20. Gullstrand, A.: Allgemeine Lösung des statischen Einkörperproblems in der Einsteinschen Gravitationstheorie. Arkiv för Matematik, Astronomi och Fysik **16**, 1 (1922)
21. Haláček, J., Ledvinka, T.: The analytic conformal compactification of the Schwarzschild spacetime. Class. Quantum Gravity **31**, 015007 (2014)
22. Hannam, M., Husa, S., Ohme, F., Brügmann, B., Murchadha, N.Ó.: Wormholes and trumpets: Schwarzschild spacetime for the moving-puncture generation. Phys. Rev. D **78**, 064020 (2008)
23. Kruskal, M.D.: Maximal extension of Schwarzschild metric. Phys. Rev. **119**, 1743 (1960)
24. Lemaître, G.: L'Univers en expansion. Annales de la Société Scientifique de Bruxelles **A53**, 51 (1933)
25. Minguzzi, E.: Lorentzian causality theory. Living Rev. Relativ. **22**, 3 (2019)
26. Minguzzi, E., Sánchez, M.: The causal hierarchy of spacetimes. Recent developments in pseudo-Riemannian geometry, ESI Lectures in Mathematics and Physics, 299 (2008)
27. Nordström, G.: On the energy of the gravitational field in Einstein's theory. Koninklijke Nederlandsche Akademie van Wetenschappen Proceedings **20**, 1238 (1918)
28. O'Neill, B.: Semi-Riemannian Geometry with Applications to Relativity. Academic Press (1983)
29. Painlevé, P.: La mécanique classique et la théorie de la relativité. Comptes Rendus de l'Académie des Sciences **173**, 677 (1921)
30. Reimann, B., Brügmann, B.: Maximal slicing for puncture evolutions of Schwarzschild and Reissner-Nordström black holes. Phys. Rev. D **69**, 044006 (2004)
31. Reinhart, B.L.: Maximal foliations of extended Schwarzschild space. J. Math. Phys. **14**, 719 (1973)
32. Reissner, H.: Über die Eigengravitation des elektrischen Feldes nach der Einsteinschen Theorie. Annalen der Physik **355**, 106 (1916)
33. Röken, C.: The massive Dirac equation in the Kerr geometry: separability in Eddington–Finkelstein-type coordinates and asymptotics. Gen. Relativ. Gravit. **49**, 39 (2017)
34. Röken, C.: Kerr isolated horizons in Ashtekar and Ashtekar–Barbero connection variables. Gen. Relativ. Gravit. **49**, 114 (2017)
35. Schindler, J.C., Aguirre, A.: Algorithms for the explicit computation of Penrose diagrams. Class. Quantum Gravity **35**, 105019 (2018)
36. Schwarzschild, K.: Über das Gravitationsfeld eines Massenpunktes nach der Einsteinschen Theorie. Sitzungsberichte der Königlich Preussischen Akademie der Wissenschaften **7**, 189 (1916)
37. Smarr, L., York Jr., J.W.: Kinematical conditions in the construction of spacetime. Phys. Rev. D **17**, 2529 (1978)
38. Stephani, H., Kramer, D., MacCallum, M., Hoenselaers, C., Herlt, E.: Exact Solutions of Einstein's Field Equations. Cambridge University Press, Cambridge (2009)
39. Szekeres, G.: On the singularities of a Riemannian manifold. Publ. Math. Debr. **7**, 285 (1960)
40. Wald, R.M.: General Relativity. University of Chicago Press, Chicago (1984)
41. Wald, R.M., Iyer, V.: Trapped surfaces in the Schwarzschild geometry and cosmic censorship. Phys. Rev. D **44**, R3719 (1991)
42. Walker, M.: Block diagrams and the extension of timelike two-surfaces. J. Math. Phys. **11**, 2280 (1970)